Pis'ma v ZhETF, vol. 85, iss. 1, pp. 46 – 51

The influence of different impurity atoms on $1/f^{\alpha}$ tunneling current noise characteristics on InAs(110) surface

A. I. Oreshkin[+1)], *V. N. Mantsevich*[+], *N. S. Maslova*[+], *D. A. Muzychenko*[+], *S. I. Oreshkin*[+*], *V. I. Panov*[+], *S. V. Savinov*[+], *P. I. Arseev*[△]

[+]*Moscow State University, Department of Physics, 119992 Moscow, Russia*

[*]*Sternberg Astronomical Institute, Moscow State University, 119992 Moscow, Russia*

[△]*Lebedev Physical Institution, 119991 Moscow, Russia*

Submitted 20 November 2006

We report the results of UHV STM investigations of tunneling current noise spectra in vicinity of individual impurity atoms on the InAs(110) surface. It was found out that the power law exponent of $1/f^{\alpha}$ noise depends on the presence of impurity atom in the tunneling junction area. This is consistent with proposed theoretical model considering tunneling current through two state impurity complex model system taking into account many-particle interaction.

PACS: 68.37.Ef, 71.55.Eq

Up to now the typical approach to $1/f^{\alpha}$ noise problem consists of "by hand" introducing of the random relaxation time τ for two-state system with the probability distribution function A/τ_0^{α}. Therefore the averaged over τ_0 noise spectra of two-states system has power law singularity. But the physical nature and the microscopic origin of such probability distribution function in general is unknown. Although the current noise gives a basic limitation for the performance of scanning tunneling microscope, only the limited number of works was devoted to study $1/f^{\alpha}$ noise. Park et al. [1] and Stoll et al. [2] have analyzed the STM data obtained above the surface of pyrolytic graphite. The power low exponent α equal to about 1.4 has been determined in [2].

In [3] Moller, Esslinger and Koslowski have investigated the noise of tunneling current at zero bias voltage. The measurements were carried out at UHV conditions at base pressure $5\cdot10^{-11}$ torr. The authors have demonstrated that at zero bias voltage the $1/f^{\alpha}$ component of noise in the tunneling current vanishes and white noise becomes dominant. Tiedje et al. [4] have found the $1/f^{\alpha}$ dependence of the current noise in STM experiments on graphite in ambient conditions. They attributed this effect to fluctuations induced by adsorbates in tunneling junction area.

In [5] the fluctuations of tunneling barrier height have been investigated. The experiments have been performed under UHV conditions on graphite and gold samples using PtIr tips. From these measurements the authors have concluded that the intensity of barrier height fluctuations correspond to the intensity of tunneling current $1/f^{\alpha}$ noise in the frequency range from 1 to 100 Hz. The physical phenomena which govern the $1/f^{\alpha}$ tunneling current noise fluctuations are discussed in [5 – 7].

Coulomb blockade as one of the sources of $1/f^{\alpha}$ noise generation is considered in [6]. The other possible mechanism is the process of atomic adsorption/desorption on the sample/tip surface in the region of tunneling contact [5].

In [7] the $1/f^{\alpha}$ tunneling current noise is explained in terms of surface diffusion of molecules adsorbed in the tunneling contact area.

To the best of our knowledge tunneling current noise STM measurements were performed only for relatively simple surfaces like gold, graphite etc. Our main goal was to clarify the *microscopic* origin of $1/f^{\alpha}$ noise. The main question in this context is how the different impurity atoms on the surface or subsurface layers and the surface defects are influencing tunneling current noise spectra.

Our STM measurements have been conducted on the clean (110) surface of InAs semiconductor compound with different chemical doping. Because in principle we need the presence of impurity atoms near the surface, for our experiments there is only one way of surface preparation, namely *in situ* cleavage [8, 9]. According to our experience even soft annealing of the sample at 600 K or ion beam cleaning at 1 keV lead to complete disappearance of doping atoms from subsurface layers.

The tunneling current spectra measurements have been done with the use of specially designed experimen-

[1)]e-mail: oreshkin@spmlab.phys.msu.su

tal setup (including both hardware and software parts), which was incorporated into our existing UHV STM "Omicron" system. Test experiments have shown that the tunneling current noise spectra are "colored" in undesirable way if STM feedback loop is turned on. At the same time in our experiments we need to go to less then 1 Hz in frequency domain, and therefore our tunneling current noise measurements are rather long. The experimental run for one curve lasts for at least 100 seconds. If STM feedback loop is interrupted, there is no way during all this time to maintain the mean value of tip-sample separation (which obviously should stay constant) except for high mechanical stability, low level of external vibrations and the whole UHV chamber being in thermally stable state. Only if all the mentioned demands are fulfilled and, besides this, the quality of STM images for selected surface is good enough, tunneling current noise measurements can be started.

InAs clean surface was prepared using *in situ* sample cleavage [8, 10]. The main advantage of this method is that the impurity atoms *do not* leave (see above) the surface layers. The impurity atoms in few subsurface layers can be imaged by STM [11].

We have used specially prepared InAs slabs ($2 \times 2 \times 4$ mm), which were cleaved *in situ* in UHV conditions. In the first set of experiments the S doped InAs (n-type bulk conductivity) single crystals were investigated. The chemical doping concentration was $1.5 \cdot 10^{18}\,\mathrm{cm}^{-3}$. In the second set of experiments the Mn doped InAs (p-type bulk conductivity) single crystals were investigated. The chemical doping concentration was $1.4 \cdot 10^{16}\,\mathrm{cm}^{-3}$. In all our measurements the tunneling bias voltage was applied to the sample, while the STM tip was virtually grounded. The presented results were obtained with a tungsten STM tips. During the sample cleavage the pressure in the UHV chamber was always lower than $1 \cdot 10^{-10}$ torr.

To properly select the set point for the STM tunneling current noise measurements we have performed the spatially resolved tunneling spectroscopy experiments. To maintain high signal to noise ratio these experiments were carried out in the current imaging tunneling spectroscopy (CITS) mode [12]. Some details concerning the data treatment can be found in [13]. The slice of two-dimensional array of $I(V)$ curves at certain value of bias voltage represents the spatial distribution of tunneling current at fixed tip-sample separation (current image). These current images give information complementary to the information which is contained in normal constant current STM (topography) image. In particular the contrast of some specific feature on the surface can be opposite on the current and on the topography STM images [13].

Because we are interested in tunneling current noise characteristics above defect free area as compared to the region of impurity atom we used the following procedure of the bias set point selection. We chose the bias voltage for current noise measurements at which the contribution from dopant atom on current image has its maximum. This means that the spot on current image caused by the presence of dopant atom is the most bright. Interesting to note that in cases of InAs_S and $\mathrm{InAs}_{\mathrm{Mn}}$ the bright spot on current image is clearly visible in wide bias voltage range approximately corresponding to the band gap range.

The typical high resolution filled states STM images of S and Mn individual impurities on the InAs(110) surface are shown on Fig.1a and Fig.2a correspondingly.

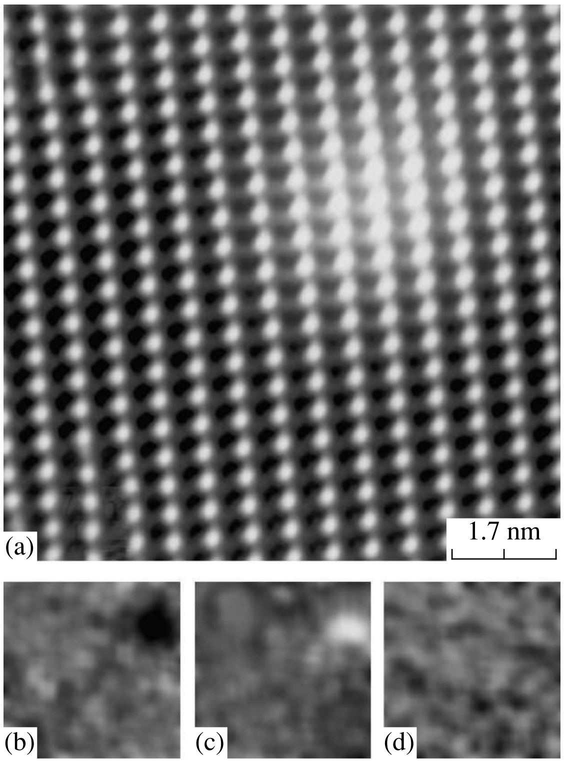

Fig.1. (a) High-resolution STM topographic image of S-dopant atom on the InAs(110) surface [$V_s = -1.16$ V, $I = 30$ pA]; The current image of S dopant atom on InAs(110) surface at (b) -0.91; c) -0.20 V; d) 0.46 V bias voltage. Scan area is 10×10 nm

Let us note, that both dopant atoms look on the occupied states STM images as round protrusions approximately 1 Å in height. The localization radius can also be estimated from STM images. In both cases it roughly

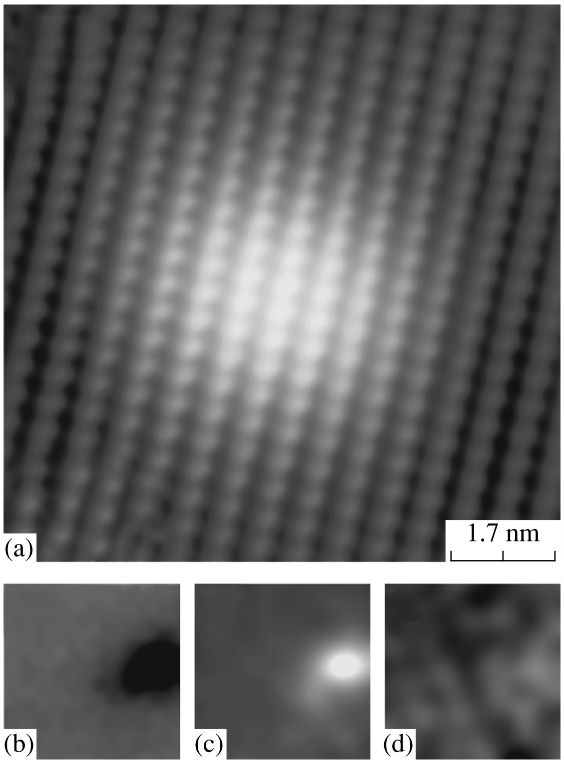

Fig.2. (a). High-resolution STM topographic image of Mn-dopant atom on the InAs(110) surface [V_s = 0.77 V, I = 30 pA]; The current image of Mn dopant atom on InAs(110) surface at (b) −1.00; (c) 0.15 V; (d) 0.48 V bias voltage. Scan area is 12.6 × 12.6 nm

equals to 40 Å providing high residual conductivity of our samples.

The current images of S dopant atom on the InAs(110) surface at different values of bias voltage are shown on Fig.1b, c, d. The most remarkable contribution from dopant atom to the current image occurs at −0.2 V bias voltage (Fig.1c). The bright spot on the current image is visible in bias voltage range from −0.54 to 0.37 V (around band gap). At positive bias voltage higher then 0.37 and up to 1 V (conduction band range) the dopant atom does not reveal itself on the current image (Fig.1d). At negative bias voltage in the range from −0.54 down to −0.73 V (valence band range) the impurity S atom is not visible on the current image. The typical current image of the impurity S atom for the bias voltage in the range from −0.73 down to −1 V is depicted on Fig.1b.

The behavior of Mn dopant atom on the InAs(110) surface is slightly different from the behavior of S impurity atom partially due to the fact that in our case $InAs_{Mn}$ has *p*-type of bulk conductivity. The current images of Mn dopant atom on the InAs(110) surface at different values of bias voltage are shown on Fig.2b, c, d. The most remarkable contribution from dopant atom to the current image occurs at 0.15 V bias voltage (Fig.2c). The bright spot on the current image is visible in bias voltage range from −0.13 to 0.42 V (around band gap). At positive bias voltage higher then 0.42 and up to 1 V (conduction band range) the dopant atom does not reveal itself on the current image (Fig.2d). At negative bias voltage in the range from −0.13 down to −0.27 V (valence band range) the impurity Mn atom is not visible on the current image. The typical current image of the impurity Mn atom for the bias voltage in the range from −0.27 down to −1.5 V is depicted on Fig.1b.

Based on this analysis the following set points values V_s for tunneling current noise measurements were chosen: $V_s = -0.2$ V for $InAs_S$, $V_s = +0.15$ V for $InAs_{Mn}$. The tunneling current value used for feedback stabilization of the tip-sample gap is equal 30 pA in all cases. The experimental procedure of the tunneling current noise measurement consists of eight steps and is described below.

1. The sample cleavage, the STM tip approach, about 6 hours of waiting to rich the stable state for the whole UHV system.

2. The search of isolated impurity atom on the InAs(110) surface by means of STM imaging. The acquisition of high resolution (∼ 50 × 50 Å) STM image of surface in vicinity of dopant atom.

3. The measurement of CITS tunneling spectroscopy in the surface region around dopant atom.

4. An analysis of the current images to find the appropriate value of bias voltage set point for the current noise measurements.

5. The positioning of STM tip right above the impurity atom or the defect free surface area with the bias voltage determined above in 4. Because the relative displacement of the STM tip is small, the effects caused by piezo manipulator creep are almost negligible. Therefore only a few minutes are needed for stabilization.

6. The interruption of the feedback loop for the time necessary to acquire the data of time domain sample of the tunneling current $I(t)$.

7. The switching on of the feedback loop.

8. The control acquisition of high resolution (∼ 50 × 50 Å) STM image of surface in vicinity of the dopant atom.

It is important to note that input stage of our tunneling current preamplifier built with Burr-Brown OPA602 operational amplifier does not limit the resolution of our measurements [14]. When tunneling bias voltage is zero or the STM tip is far from the surface (no tunneling current flows) we could not observe any sights of $1/f^{\alpha}$

component in the noise spectra, which is consistent with results of [3].

The results of the tunneling current noise measurements on (110) surface of S and Mn doped semiconductor compound InAs are presented on Fig.3 and Fig.4 respectively. The tunneling current noise spectra are

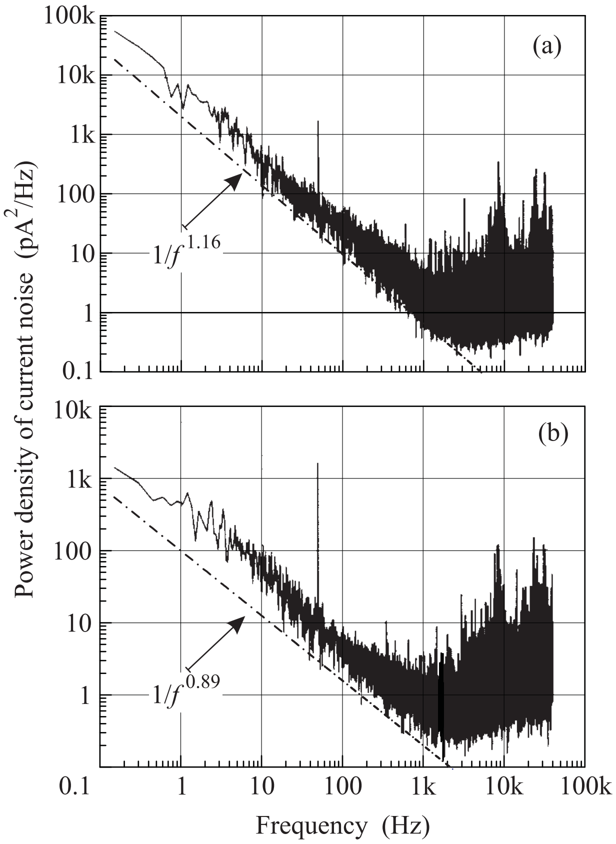

Fig.3. Power spectrum of tunneling current measured above (a) individual S-dopant atom; (b) defect free surface; $V_s = -0.2$ V, $I = 30$ pA

shown in double logarithmic scale for clarity. The $1/f^{\alpha}$ dependence is clearly evident, the cut off frequency of $1/f^{\alpha}$ noise component is approximately 1 kHz. The dashed line on Fig.3, 4 shows the linear approximation of the current noise spectrum curve obtained by least-mean-squares method (LMS) in the frequency range from 0.1 Hz to ~ 1 kHz (cut off frequency).

Some important points from our results can be emphasized. We have found that both for $InAs_S$ and $InAs_{Mn}$ the power low exponent is different for measurements above defect free surface area and above impurity atom.

For $InAs_S$ the power low exponent α measured above clean surface is equal to 0.89 whereas above dopant atom it has value 1.16. For $InAs_{Mn}$ the power low exponent α

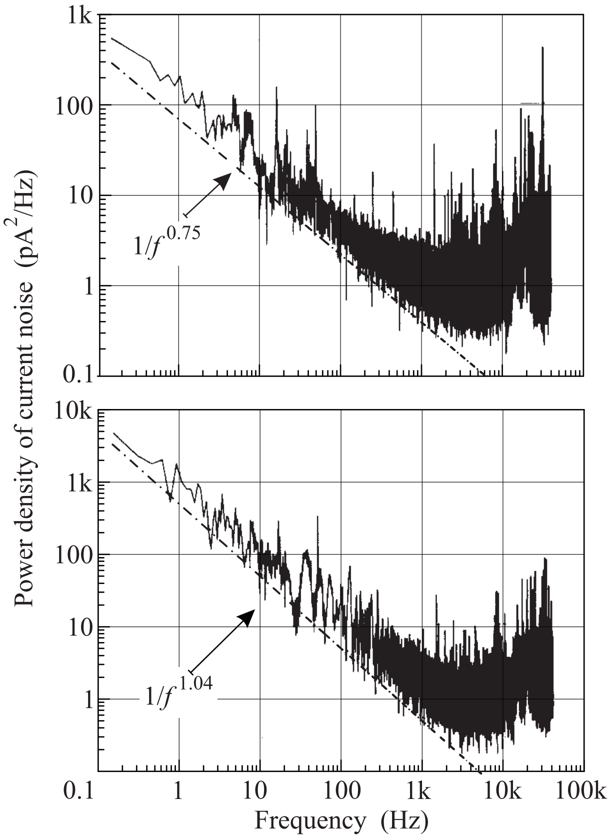

Fig.4. Power spectrum of tunneling current measured above a) individual Mn-dopant atom; b) defect free surface; $V_s = 0.15$ V, $I = 30$ pA

measured above clean surface is equal to 1.04 whereas above dopant atom it has value 0.75.

One can see the difference in the behavior of the power low exponent in cases of $InAs_S$ and $InAs_{Mn}$. While moving from the impurity atom to the clean surface α is decreasing for $InAs_S$ sample (Fig.3a,b). The opposite situation was observed for $InAs_{Mn}$ surface. The α is increasing when moving away from dopant atom (Fig.4a,b).

As it was shown in [15, 16] sudden switching "on" and "of" Coulomb potential of impurity due to tunneling transitions of impurity electrons to the leads results in power lower singularities of $I(V)$ curves. The sign of power low exponent is determined by the sign of impurity charge. In the spatial distribution of tunneling current one can see switching "on" and "of" of the impurity atoms at certain values of applied bias, which is connected with power low singularity of tunneling current at threshold voltage. Such singular behavior of tunneling current was obtained by re-normalization of tunneling matrix element by switched "on" and "of" Coulomb potential of charged impurities. In calculating current noise spectra just the same re-normalization of tunneling vertex leads to its power law behavior. The model system (Fig.5) can be described by hamiltonian $\widehat{H}$:

$$\widehat{H} = \widehat{H}_0 + \widehat{H}_T + \widehat{H}_{\text{int}},$$

$$\widehat{H}_0 = \sum_k (\varepsilon_k - eV) c_k^+ c_k + \sum_p \varepsilon_p c_p^+ c_p + \sum_{i=1,2} \varepsilon_i a_i^+ a_i,$$

$$\widehat{H}_T = \sum_{k,i} T_{ki} c_k^+ a_i + \sum_{p,i} T_{pi} c_p^+ a_i + T \sum_{i \neq j} a_i^+ a_j + \text{h.c.},$$

$$\widehat{H}_{\text{int}} = \sum_{k,k'} W_1 c_k^+ c_{k'} a_1 a_1^+ + \sum_{k,k'} W_2 c_k^+ c_{k'} a_2 a_2^+.$$

For clean surface one should put $T_{p2} = 0$, $\varepsilon_2 = 0$, $T = 0$, $W_2 = 0$, $T_{k2} = 0$, $\varepsilon_1 = eV$, if ε_1 is connected with the tip apex state. Re-normalization of T_{k1} due to switching

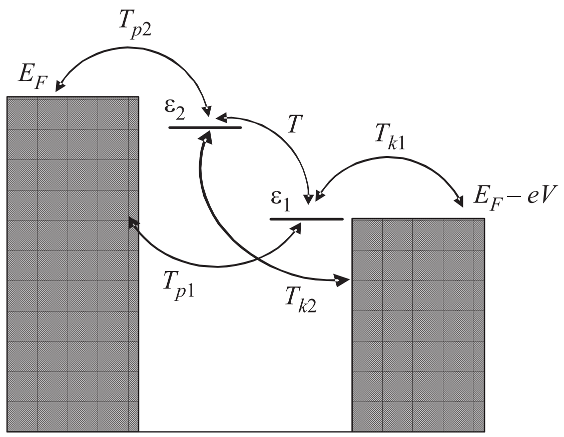

Fig.5. Schematic diagram of tunneling through states localized on impurity atom and on the STM tip apex

"on" and "of" of W_1, gives the low frequency contribution to $S(\omega)$ above clean surface:

$$S_{\text{clean}}(\omega) = \left(\frac{\xi_0}{\omega}\right)^{-W_1 \nu}.$$

Above the impurity atom, near threshold value of applied bias both tunneling vertex T_{k1} and T_{k2} should be re-normalized by switched "on" and "of" Coulomb potentials W_1 and W_2 correspondingly. The low frequency noise spectra above impurity can be estimated as:

$$S_{\text{imp}}(\omega) \sim S_1(\omega) S_2(\omega) \sim \left(\frac{\xi_0}{\omega}\right)^{-(W_1+W_2)\nu},$$

$$\alpha_{\text{imp}} = -(W_1 + W_2)\nu.$$

Tip apex is neutral, so tunneling transitions determined by T_{k1} lead to switching on Coulomb potential $W_1 < 0$ of positively charged "hole". The changes in power low exponent above the impurity atoms depends on the sign of W_2, and thus on the initial charge of impurity. For negatively charged impurity $W_2 > 0$, while for positively charged impurities $W_2 < 0$. For p-type InAs Mn atom is negatively charged, $W_2 > 0$ and

$$S_{imp}(\omega) \sim \left(\frac{\xi_0}{\omega}\right)^{(|W_1|-|W_2|)\nu},$$

$$\alpha_{\text{imp}} = (|W_1| - |W_2|)\nu;\ \alpha_{\text{clean}} = |W_1|\nu$$

$$\alpha_{\text{imp}} < \alpha_{\text{clean}}.$$

So, for p-type InAs power low exponent above Mn dopant atom is smaller compared to low frequency noise power low exponent above clean surface. The situation is opposite for n-type InAs doped by S, which is positively charged

$$S_{\text{imp}}(\omega) \sim \left(\frac{\xi_0}{\omega}\right)^{(|W_1|+|W_2|)\nu}.$$

In this case $\alpha_{\text{imp}} = (|W_1| + |W_2|)\nu$; $\alpha_{\text{clean}} = |W_1|\nu$,

$$\alpha_{\text{imp}} > \alpha_{\text{clean}}.$$

This model qualitatively describes the observed experimental results.

In conclusion, we have found that both for $InAs_S$ and $InAs_{Mn}$ the power low exponent is different for measurements above defect free surface area and above impurity atom. For $InAs_S$ the power low exponent α measured above clean surface is equal to 0.89 whereas above dopant atom it has value 1.16. For $InAs_{Mn}$ the power low exponent α measured above clean surface is equal to 1.04 whereas above dopant atom it has value 0.75. The microscopic theoretical approach taking into account many-particle interaction was proposed to model the experimental results. Sudden switching on and off of additional Coulomb potential in tunneling junction area leads to typical power law dependence for low frequency tunneling current noise spectra.

Basically the tunneling current noise measurements can give an additional information which is principle together with STM imaging and scanning tunneling spectroscopy can allow to identify the chemical nature of individual impurity atoms near the surface. But to reach this goal a lot of work still has to be done both in the fields of theory and experiment. In the present investigation we restrict ourselves to the case of noninteracting (isolated) individual impurity atoms on clean (110) surface of semiconductor compound InAs.

This work was partially supported by RFBR grants # 06-02-17076-a, # 06-02-17179-a, # 05-02-19806-MF, # 06-02-08306-OFI, president grants for scientific school

4599.2006.2 and # 4464.2006.2. Support from Samsung corporation is also gratefully acknowledged. Authors are thankful to V.V. Gubernov and A.A. Ezhov for valuable discussions.

1. S. Park AND C.F. Quate, Appl. Phys. Lett. **48**, 112 (1986).
2. E. Stoll and O. Marty, Surf. Sci. **181**, 222 (1987).
3. R. Moller, A. Esslinger, B. Koslowski, Appl. Phys. Lett. **55**, 2360 (1989).
4. T. Tiedje, J. Varon, H. Deckman, and J. Stokes, J. Vac. Sci. Technol. B **A6**, 372 (1988).
5. M. Lozanoet and M. Tringides, Europhys. Lett. **30**, 537 (1995).
6. K. Maeda, K. Suzuki, S. Fujita, M. Ichihara et al., J. Vac. Sci. Technol. B **12**, 2140 (1994.)
7. G.K. Zyrianov, *Low-voltage electronography*. L. (1986).
8. A. Oreshkin, A.I. Oreshkin, D.,A. Myzichenko et al., Rev. Sci. Instrum. **77**, 11, accepted for publication, (2006).
9. P.I. Arseyev, N.S. Maslova, S.V. Savinov et al., Pis'ma v ZhETF **82**, 312 (2005).
10. S. Oreshkin, A.I. Oreshkin, D.A. Myzichenko et al., *Instruments and experimental Techniques* N6, 1 (2006).
11. A. Depuydt, P.I. Arseyev, N.S. Maslova, S.V. Savinov et al., Phys. Rev. B **60**, 2619 (1999).
12. R. Wiesendanger, *Scanning probe microscopy and spectroscopy*, Cambridge University Press, 1994.
13. P.I. Arseyev, N.S. Maslova, S.V. Savinov et al., JETP Lett. **77**, 202 (2003).
14. Texas Instruments Incorporated, OPA602 data sheet, www.ti.com
15. P.I. Arseyev, N.S. Maslova, S.V. Savinov et al., JETP Lett. **76**, 287 (2002).
16. P. Nozieres and C. T. De Dominicis, Phys. Rev. **178**, 1097 (1969).